Electronic Supplementary Information

Superwetting and mechanically robust MnO_2 nanowires-reduced graphene oxide monolithic aerogels for efficient solar vapor generation

Zheng Zhang, Peng Mu, Jingxin Han, Jingxian He, Zhaoqi Zhu, Hanxue Sun, Weidong Liang and An Li*

Characterizations

The morphologies of the materials were examined by performing scanning electron microscope (SEM, JSM-6701F, JEOL, Ltd) and transmission electron microscope (TEM, Tecnai G2TF20). All TGA experiments were performed with 9-10 mg samples on thermo gravimeter analyzer (Perkin Elmer) from room temperature to 800 ^{o}C at a heating and cooling rate of 10 ^{o}C min^{-1} under nitrogen atmosphere. FTIR spectra were recorded from in the range of 4000-400 cm^{-1} using the KBr pellet technique on a Nexus 670 spectrum instrument. The X-ray diffraction (XRD) was performed on a Rigaku D/Max-2400 diffractometer with 2θ at 2° to 80°. The thermal conductivity of aerogel was investigated on flash method thermal analyzer (LFA 447, Netzsch). The UV-vis absorption was conducted at UV-vis spectrometer Lambda 750 from 200~2500 nm with an integrated sphere. Note that the integrating sphere was utilized to collect the scattered light for accurate measurement. The camera photos was recorded at Photron Fastcam Mini UX100 type high speed video camera. The compressive properties were performed by using an electrical universal material testing machine with equipped two flat-surface compression stages and a 500 N load cell (EZ-Test, SHIMADZU) at a stress rate of 5mm/min. The elemental analyse was carried out on an elemental analyzer (Elementar Vario EL). EDS measurements were carried on an FEI Talos transmission electron microscope equipped with a Super-X EDS detector and operated at an accelerating voltage of 200 kV. The Brunauer-Emmett-Teller (BET) surface areas and pore structures of the samples were measured by a micromeritics ASAP 2020 apparatus at 77.3 K, all samples were degassed at 120 ^{o}C overnight under vacuum before analysis. The infrared thermal images is obtained with an infrared camera (Thermal Imager TESTO 869, Testo SE & Co. KGaA, Germany). The contact angles was recorded with a standard contact-angle analyzer (PT-705-A, Pusite Detection Equipment Co., Dongguan, China) at room temperature. XPS spectra were obtained using a Physical Electronics 5000 VersaProbe II Scanning ESCA (XPS) Microprobe.

Solar steam generation test

The solar steam generation experiments was conducted at a lab-made, online, real-time measurement system which is composed by (1) a solar light simulator (xenon arc lamp, CEL-S500, Ceaulight) with (2) a solar filter (AM 1.5, Ceaulight), a test chamber with 80 mm in height 36 mm in diameter, (3) an analytical balance (FA 2004) (4) a computer to record the time-dependent mass change of water due to the stream generation (5) an

infrared camera (Testo 869, Germany). Light intensity was measured by a full spectrum optical power meter (CEL-NP2000-2, Beijing Education Au-light Co., Ltd.). During each test, the room temperature was maintained at 19-22 ^{o}C and the humidity was ranged from 15 and 20%.

Calculation of the energy conversion efficiency

$$\eta = \dot{m} (Lv+Q) / Pin$$

Where $\dot{m}$ is the mass flux of steam (the rate of water evaporation under the dark environment subtracted), Lv is the latent heat of water evaporation (J kg^{-1}), Q is the sensible heat of water (J kg^{-1}), and Pin is the power of the incident simulated sunlight beam. The latent heat Lv is dependent on the temperature (Ti) of the water/air interface where the vaporization occurs. It varies from 2,453 kJ kg^{-1} at 20^{o}C to 2,256 kJ kg^{-1} at 100^{o}C. The sensible heat Q is calculated from the specific heat of water and the temperature difference between the source water (Ts) and water/air interface (Ti). The temperature of the water/air interface (Ti) greatly affects the values of both latent heat Lv and sensible heat Q, and therefore affects the calculation of energy efficiency.

Speaking of latent heat Lv in this formula, there is currently no fixed standard for calculating efficiency. When calculating solar thermal water evaporation efficiency, part of the articles in this field always use the 2256 kJ kg^{-1} corresponding to 100^{o}C as the latent heat. There are still some articles that are consistent with our calculation method, the latent heat varies from 2,453 kJ kg^{-1} at 20^{o}C to 2,256 kJ kg^{-1} at 100^{o}C. This may cause the final solar thermal water evaporation efficiency to be slightly higher than the former. It is not uncommon for this kind of efficiency to exceed 100% of the literature (such as Joule, 2018, 2, 1171-1186, Advanced Sustainable Systems, 2017, 1, 1700046 and J. Mater. Chem. A, 2018, 6, 17212-17219). We will focus our future research on theoretical heat balance and how to reduce heat loss during evaporation.

Referring to the details of the support of these literatures, the commonality of these literatures is that the way to calculate energy conversion efficiency is the same as our work. The energy conversion efficiency of these documents reaches 100% or exceeds 100% without considering heat loss. This violates the law of conservation of energy. Accurate calculation of heat loss is a difficult problem in this field, and there is currently no standard for calculating energy conversion efficiency and accurate heat loss calculation standards. We will focus on this point in the next step of our work.

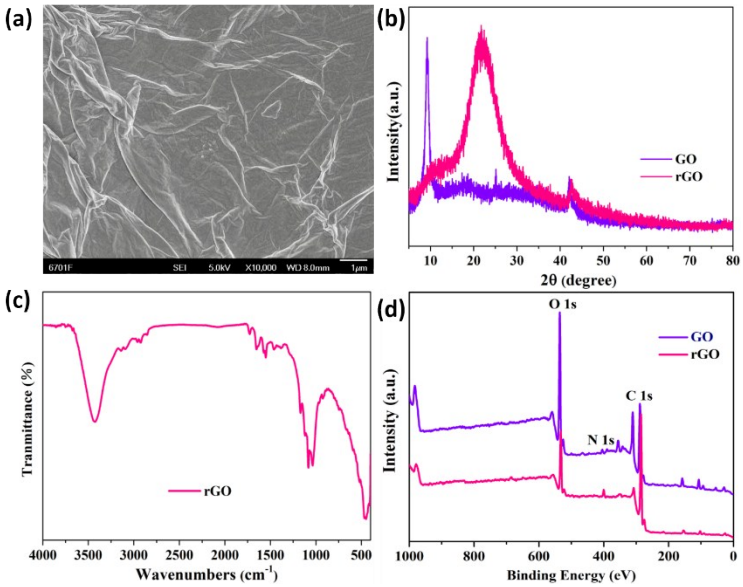

Fig. S1 (a) SEM images of the GO we prepared; **(b)** XRD spectra of the GO and rGO; **(c)** FTIR spectrum of rGO; **(d)** XPS spectra of GO and rGO.

It is clear from the Fig. S1d, the reduction effect is clear since the content of oxygen (O) atoms of rGO significantly reduces compared with GO. Indicates that GO was successfully reduced.

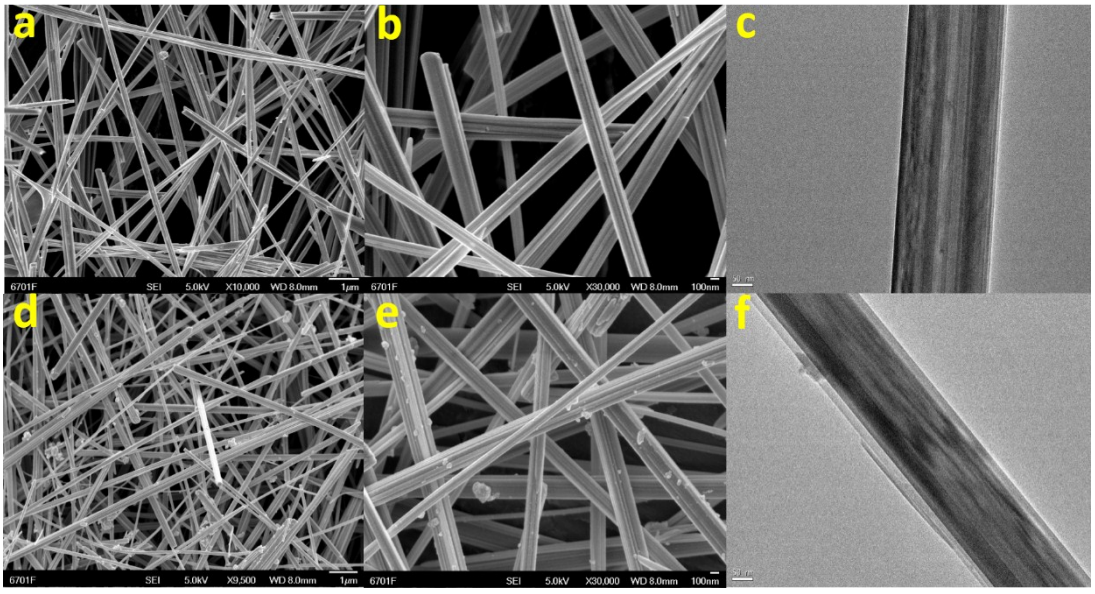

Fig. S2 (a, b) SEM images of the MnO_2 nanowires before hydrophilic treatment; **(c)** TEM images of the MnO_2 nanowires before hydrophilic treatment; **(d, e)** SEM images of the MnO_2 nanowires after hydrophilic treatment; **(f)** TEM images of the MnO_2 nanowires after hydrophilic treatment.

Compared with the nanowires before and after superhydrophilicity, the SEM image is not obvious, and the distinct coating can be seen from the TEM image.

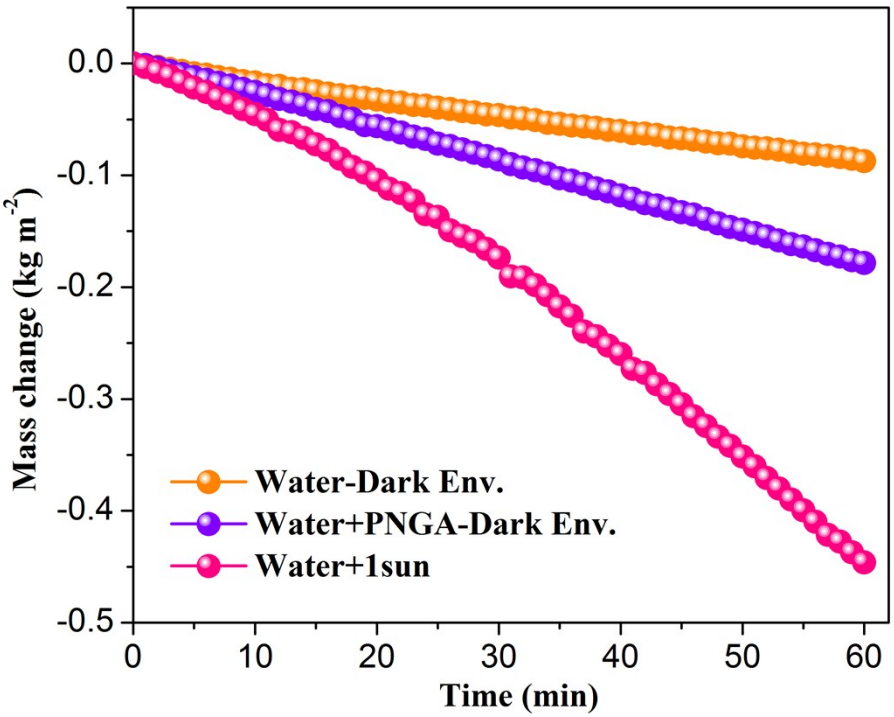

Fig. S3 Evaporation under dark condition. The evaporation rate of water under dark conditions and under solar irradiation of 1 kW m^{-2}. The absorption of water and its temperature increase causes a significant enhancement in evaporation.

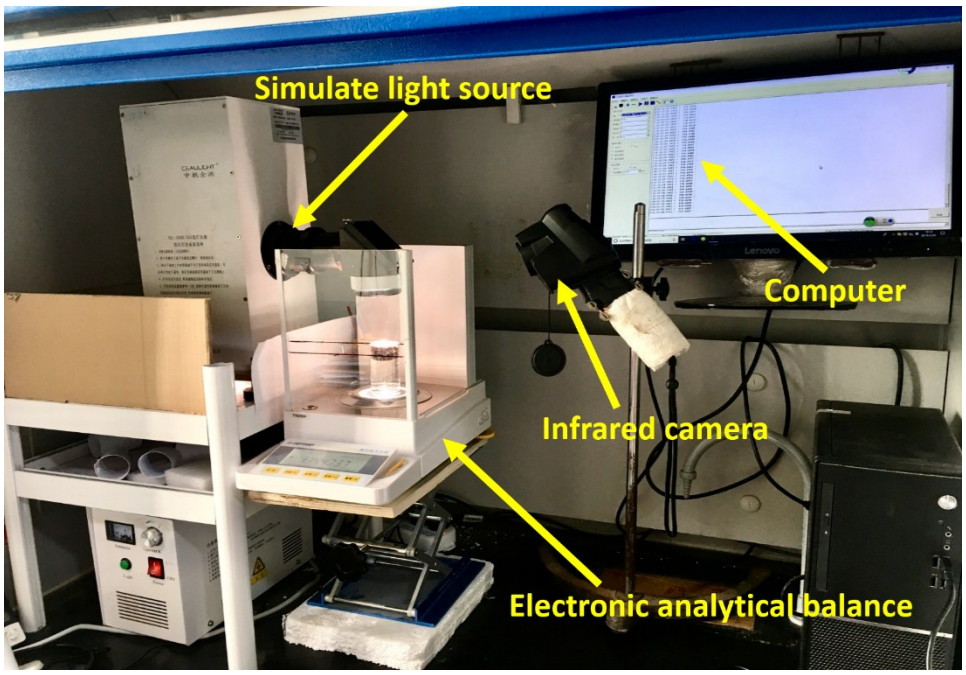

Fig. S4 Schematic diagram of the equipments we used for solar steam generation performance testing.

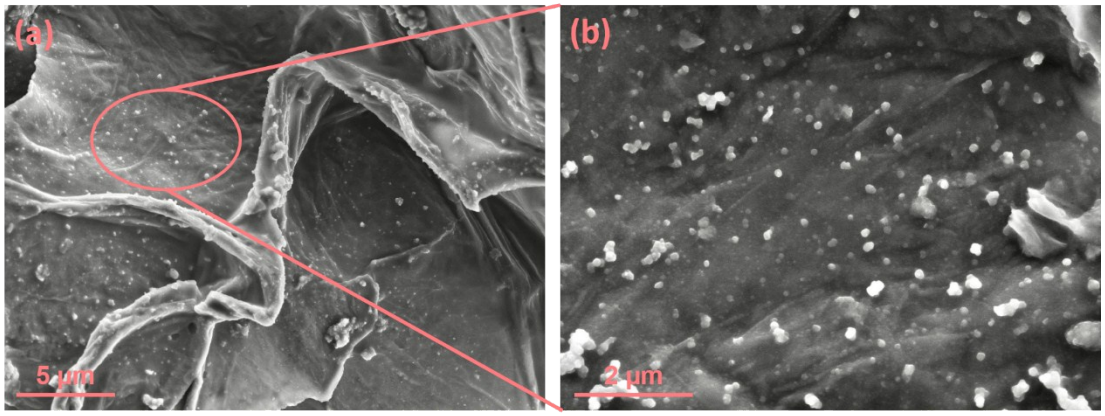

Fig. S5 SEM images of PNGA aerogel's surface under different magnification, Polypyrrole particles on graphene sheets can be clearly seen.

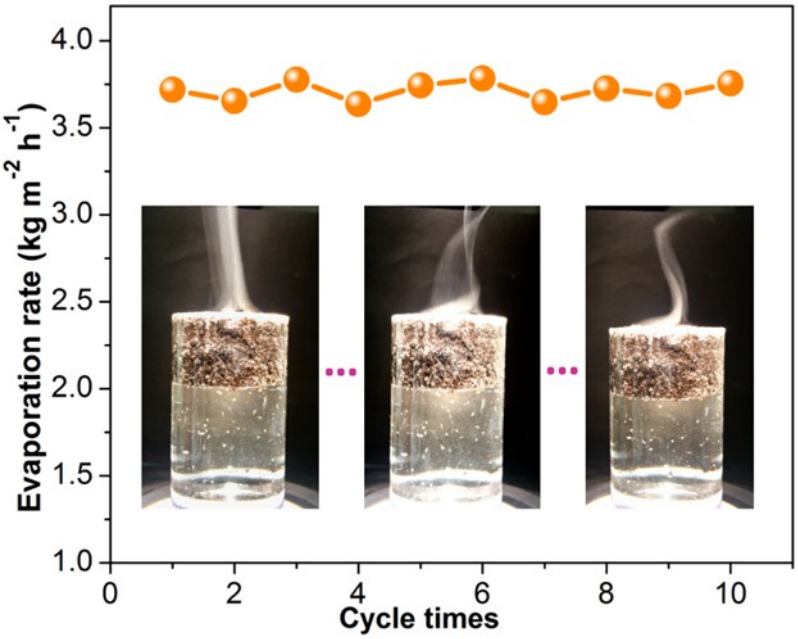

Fig. S6 Evaporation rates of the recycled PNGA aerogel under 3.0 kW m^{-2}.

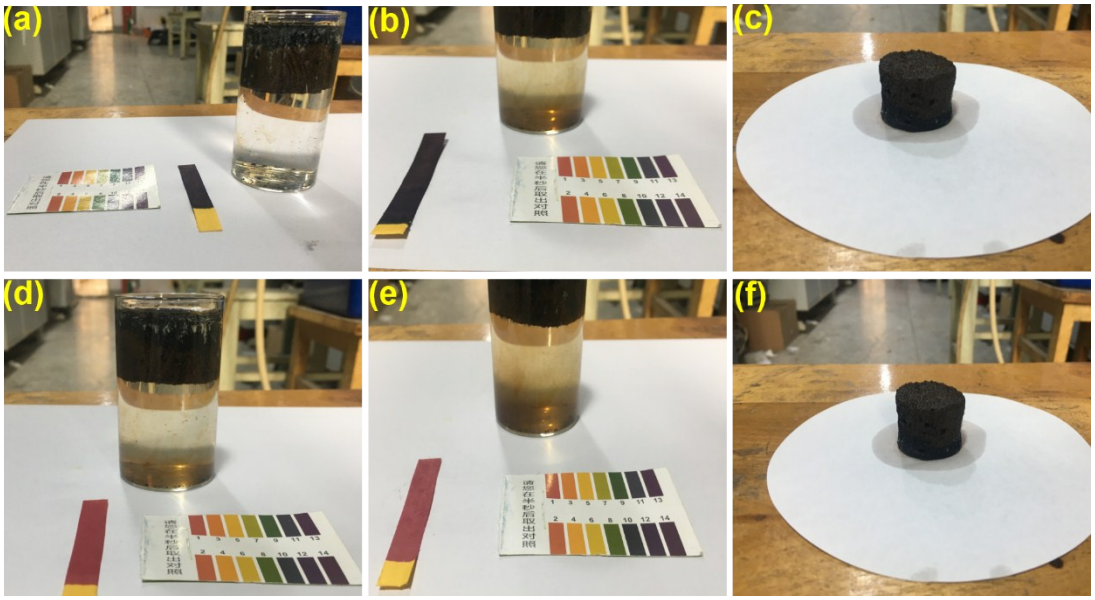

Fig. S7 (a,b,c) Photograph of our aerogel material soaked in 0.1 mol/L NaOH, (a, b, c respectively represent the picture just immersed, immersed for half an hour and taken out). (d,e,f) Photograph of our aerogel material soaked in 0.1 mol/L HCl, (a, b, c respectively represent the picture just immersed, immersed for half an hour and taken out).

Because our raw materials are manganese dioxide nanowires and graphene oxide, they do not react with hydrochloric acid and sodium hydroxide at normal temperature and pressure. Therefore, our aerogel materials have a certain resistance to acid and alkali corrosion, making them more likely to survive in harsh environments.

We compared the evaporation rate in this article with that in other literatures and summarized them in Table S1. All data compared represent the highest efficiency value under 1.0 kW m^{-2} radiation in the literatures. Compared with these literatures, our work greatly simplifies the preparation process while maintaining competitive evaporation performance, opens up possibilities for large-scale preparation, and innovatively introduces the concept of super-hydrophilic coatings into solar steam generation.

Table S1 Solar tests results compared with other literatures.

Data source	Evaporation flux (kg m^{-2} h^{-1})	Energy conversion efficiency (%)
This article	1.587	93.8
Advanced Energy Materials, 2019, 9, 1802158	1.5936	93.4
Journal of Materials Chemistry A, 2018, 6, 18183-18190	1.3992	81
Journal of Materials Chemistry A, 2019, 7, 9673-9679	1.3752	82.4
ChemSusChem, 2019, 12, 426-433	1.205	73.3
Nano Energy, 2019, 56, 708-715	1.63	94.9
Journal of Materials Chemistry A, 2018, 6, 12267-12274	1.54	88.8
Advanced Functional Materials, 2018, 28, 1707134	1.15	80
Advanced materials, 2017, 29, 1700981	1.25	85.6
Advanced materials, 2017, 29, 1604031	1.622	83
Advanced materials, 2017, 29, 1606762	1.475	78
Chemical Science, 2018, 9, 623-628	1.1687	80.5
Journal of Materials Chemistry A, 2017,5, 18397-18402	1.13	78
Joule, 2018, 2, 1171-1186	2.04	100

Heat Loss Analysis

According to the literatures (Adv. Mater. 2017, 29, 1700981; Adv. Mater. 2017, 29, 1604031 and Chem. Sci., 2018, 9, 623-628), The input heat flux is 1 kw/m^2, we take PNGA sample under 1 sun irradiation as an example. The heat loss of the evaporator contains (1) radiation, (2) conduction and (3) convection. The calculation details of heat loss are shown below.

Calculation of heat losses:

Radiation:

The radiation loss was analyzed by Stefan-Boltzmann equation. The room temperature is about 20^{o}C. Supposing the evaporator has a maximum emissivity of 1.

$$\Phi = \varepsilon A\sigma(T_1^4-T_2^4) \qquad (1)$$

Where Φ is heat flux (W m^{-2}), ε denotes emissivity, A is the surface area of the absorber facing the sun (0.00079011m^2), σ is the Stefan-Boltzmann constant (5.67×10^{-8} W m^{-2} K^{-4}, T_1 is the surface temperature of the evaporator after stable steam generation under one-sun illumination equal to 316.15 K. T_2 is the initial surface temperature of the evaporator before illumination equal to 293.15 K. According to the equation (1), we can calculate that the radiation heat loss is ～1.3% of all received solar energy.

Conduction:

The heat loss of conduction is the heat from absorber to warm bulk water and was calculated according to the following equation.

$$Q=Cm\Delta T \qquad (2)$$

Where Q is the heat energy, C denotes the specific heat capacity of pure water (4.2 kJ $^oC^{-1}$ kg^{-1}), m represents the weight of bulk water and ΔT is the increased temperature of the bulk water after stable steam generation. In our experimental, m=120 g, ΔT≈1.4°C. Therefore, the calculated heat loss of conduction is ～6% of all received solar energy.

Convection:

The heat loss of convection is caused by the air flowing and was analyzed by the following Newton' law of cooling.

$$Q= hA\Delta T \qquad (3)$$

Where Q is the heat energy, h is the natural convection heat transfer coefficient (～5-10 W m^{-2} K^{-1}). A is the surface area of the absorber facing the sun (0.00079011m^2). ΔT is different between the room temperature and the surface temperature of the evaporator. Based on the above equation, the heat loss of convection of the evaporator is ～3.1% of all received solar energy.

As to the conduction to the underlying water, we estimate it to be 6% according to a very similar solar-thermal evaporation system (Nat. Commun., 2014, 5, 4449), where the conductive heat loss is at most 6% at different solar concentrations (from 1 kW m^{-2} to 3 kW m^{-2}). Since the thermal conductivity of our PNGA sample surface (0.21882 W m^{-1} K^{-1}) is much lower than that of the above paper (0.93 W m^{-1} K^{-1}), the conductive heat loss of our system should be no more than 6%. For the calculation of heat loss, only a rough range can be estimated as much as possible and cannot be accurately estimated.